Induced-charge electrophoresis of ideally polarizable particle pairs

S. Oren and I. Frankel
Faculty of Aerospace Engineering, Technion – Israel Institute of Technology, Haifa 3200003, Israel

(Received 26 March 2020; accepted 7 August 2020; published 24 September 2020)

We study the planar two-dimensional relative induced-charge electrophoretic (ICEP) motion of a pair of identical, ideally polarizable circular cylindrical microparticles carrying no net charge and freely suspended in an unbounded electrolyte solution under a uniform steady (DC) external electric field acting in an arbitrary direction relative to the instantaneous orientation of their line-of-centers (LOC). Within the framework of the thin electric-double-layer (EDL) limit and sufficiently weak fields description of particle paths is obtained via integration of the quasisteady kinematic equations of motion based on the instantaneous geometric configuration. Owing to the inherent nonlinearity of the ICEP mechanism, interaction of the effects of external-field components parallel and perpendicular, respectively, to the LOC results in its rotation which, in turn, determines that particles undergo transient pairing eventually moving apart in the general direction perpendicular to the external field. Dielectrophoresis is demonstrated to only have a secondary effect on the resulting motion.

DOI: 10.1103/PhysRevFluids.5.094201

I. INTRODUCTION

When an ideally polarizable (conducting) initially uncharged circular cylinder freely suspended in an unbounded electrolyte solution is subject to a uniform external field, it instantaneously polarizes acquiring surface-charge distribution so as to maintain zero electric field within the conducting solid. At the same time a diffuse cloud of counterions forms within the adjacent fluid via Ohmic electromigration from the bulk solution, thereby creating an induced electric double layer (EDL). When steady state is established, the field lines become tangent to the solid (as the EDL is no longer being charged). The action of the external field on its own-induced EDL gives rise to a symmetric induced-charge electro-osmotic flow (ICEO) [1].

Owing to the perfect symmetry, the resultant force and torque generated by the above mechanism on the circular-cylindrical particle both vanish under a uniform external field and the particle thus remains stationary. Induced-charge electrophoretic (ICEP) motion can, however, result from asymmetry of material properties (e.g., as in Janus particles), or of particle shape [2,3]. Asymmetry may also be introduced by the presence of boundaries, e.g., a planar wall [4,5] or adjacent particles [6–10].

Beyond fundamental theoretical interest, the relative motion of particle pairs is of considerable relevance to suspension dynamics. Thus, Saintillan's analysis [7] of pairwise hydrodynamic interactions serves to obtain macroscale statistical description of multiparticle semidilute suspensions of rodlike [6] and spherical [8,9] particles; pairing events may represent the precursor of chaining, which is important in suspension stability and micro- and nanoparticle manipulation in a variety of material-processing scenarios [11].

We here consider the planar two-dimensional (2D) relative motion of a pair of identical ideally polarizable, circular-cylindrical particles freely suspended in an unbounded electrolyte solution under a uniform steady (DC) external electric field, within the framework of the thin-EDL limit

and assuming sufficiently weak fields. A similar configuration was addressed by Kang [12] who studied by means of finite-volume numerical simulations the motion of a pair of cylinders confined in a finite 'electrically neutral' square cavity under a uniform DC external field. More recently, Feng, Wong, and Marcos [13] analyzed the pair motion in an unbounded domain under a uniform DC external field, yet only for the symmetric cases of fields acting either parallel or perpendicular to the particles line of centers (LOC). In both cases, owing to symmetry, particles motion is limited to a symmetric translation along this line. However, owing to the inherent nonlinearity, the pair motion under an arbitrarily oriented field cannot be obtained via superposition of these particular cases. The present study thus aims at analyzing the pair motion under a uniform DC electric field acting perpendicularly to their axes in a general direction relative to the instantaneous LOC. The rest of this contribution is organized as follows: The relevant electrochemical and hydrodynamic problems are stated in the next section and their analysis is then outlined in Sec. III. Subsequently, the relative ICEP particles velocities and the resulting paths are presented in Sec. IV and the role of the dielectrophoresis in the present problem is considered in Sec. V. Section VI provides some concluding comments.

II. STATEMENT OF THE PROBLEM

We consider a pair of identical ideally-polarizable (conducting), circular-cylindrical particles (radii a'; primes hereinafter denoting dimensional quantities), whose centers are instantaneously a distance $2b'$ apart (as schematically depicted in Fig. 1). The particles are freely suspended in an unbounded electrolyte solution (viscosity μ' and electric permittivity ε'), subject to a uniform and constant (DC) external electric field $\boldsymbol{E}_{\mathbf{0}}'$ making an angle θ relative to the instantaneous orientation of the particles LOC. The following dimensionless formulation is (initially) based on the length scale $c'[= (b'^2 - a'^2)^{\frac{1}{2}}]$, the electric potential $c'E_0'(E_0' = |\boldsymbol{E}_{\mathbf{0}}'|)$, the velocity $(\varepsilon' E_0'^2 c')/\mu'$ and the stress $\varepsilon' E_0'^2$.

Within the framework of the thin-EDL-limit and sufficiently weak fields the electrochemical and hydrodynamic problems decouple in the quasi-electro-neutral bulk. Thus, the harmonic electric potential, satisfies the homogeneous Neumann condition

$$\hat{\boldsymbol{n}} \cdot \nabla \Phi = 0 \quad \text{at } \boldsymbol{r} \in S_i \ (i = 1, 2), \tag{2.1}$$

where S_i $(i = 1, 2)$ denote the surfaces of the cylinders and $\hat{\boldsymbol{n}}$ are unit vectors normal to S_i directed into the fluid. At the far field we require convergence to the uniform external field

$$\nabla \Phi = - \quad \widehat{\boldsymbol{E}_{\mathbf{0}}} \quad \text{as } r \to \infty \tag{2.2}$$

with $\widehat{\boldsymbol{E}_{\mathbf{0}}}$ denoting a unit vector in the direction of the external field. In the present narrow-EDL model the electro-osmosic phenomenon is represented by the Helmholtz-Smoluchowski slip velocity, effectively imposed at the surfaces of both cylinders which, in view of Eq. (2.1), is written here

$$\boldsymbol{u}_{\boldsymbol{s}} = \zeta \nabla \Phi \quad \text{at } \boldsymbol{r} \in S_i \ (i = 1, 2), \tag{2.3}$$

where ζ is the zeta potential, i.e., the potential difference across the EDL.

The hydrodynamic problem comprises the equation of continuity

$$\mathrm{div}\boldsymbol{u} = 0 \tag{2.4}$$

and, given the small Reynolds numbers associated with microparticles, the Stokes equation

$$\nabla p = \mu \nabla^2 \boldsymbol{u}, \tag{2.5}$$

wherein $\boldsymbol{u}$ and p denote the fluid velocity and pressure, respectively. The above are supplemented by

$$\boldsymbol{u} = \boldsymbol{U_i} + \boldsymbol{\Omega_i} \times (\boldsymbol{r} - \bar{\boldsymbol{r}}_{\boldsymbol{i}}) + \boldsymbol{u}_{\boldsymbol{s_i}} \quad \text{at } \boldsymbol{r} \in S_i \ (i = 1, 2), \tag{2.6}$$

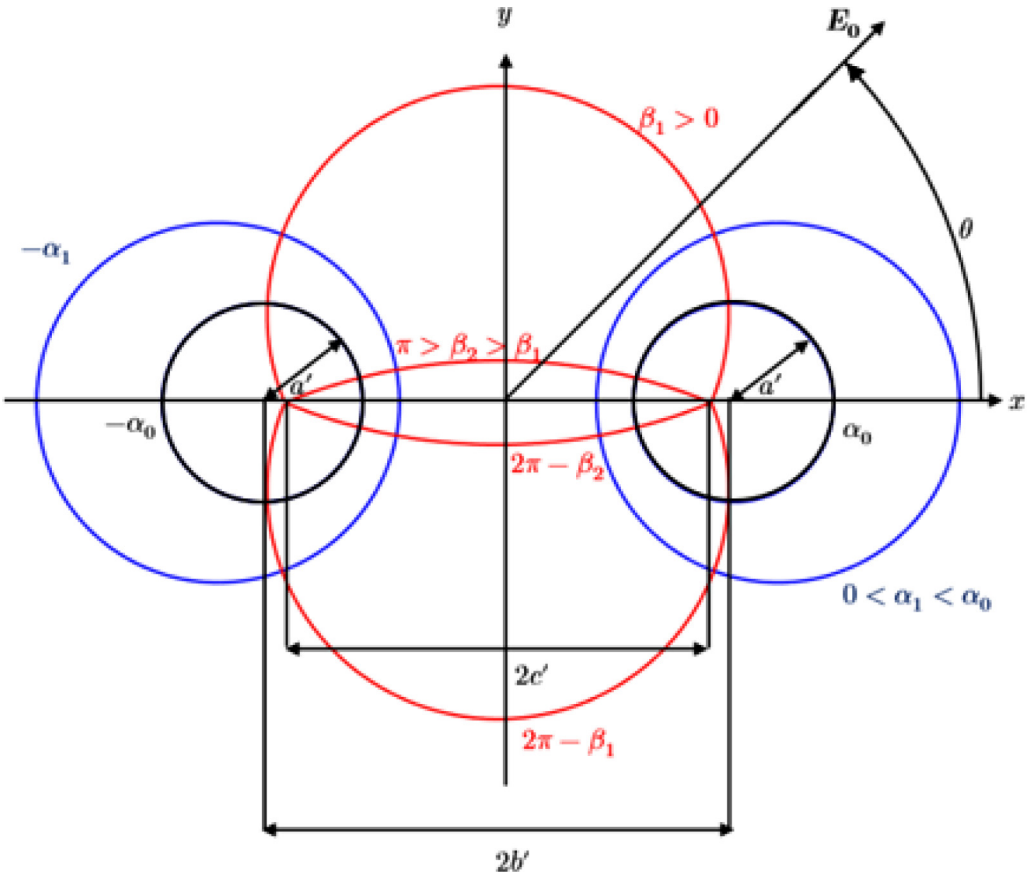

FIG. 1. Schematic definition of geometric configuration and cylindrical bipolar coordinates (α, β). Marked by the black circles are the pair of particles of radii a' centered at $(\pm b', 0)$ and subject to the uniform external field $\boldsymbol{E}_{\mathbf{0}}^{'}$. The two families of nonintersecting circles correspond to curves of constant α (with $\pm\alpha_0$ pertaining to the pair of particles). The red arcs leaning on the common chord extending between $(\pm c',\ 0)$ describe the family of constant-β curves.

at the particles surface together with the far-field attenuation condition

$$\boldsymbol{u} = 0 \quad \text{as } r \to \infty. \tag{2.7}$$

In Eq. (2.6) $\boldsymbol{U_i}$ are the translational velocities at the centers $\bar{\boldsymbol{r}}_{\boldsymbol{i}}$ of both cylinders, $\boldsymbol{\Omega_i}$ are their angular velocities and $\boldsymbol{u}_{s_i}$ are the electro-osmotic Helmholtz-Smoluchowki slip velocities. For freely suspended particles, neglecting fluid- and microparticles inertial effects, $\boldsymbol{U_i}$ and $\boldsymbol{\Omega_i}$ are to be eventually determined from the required vanishing of the resultant force

$$\boldsymbol{F} = \int_{S_i} (\boldsymbol{\Pi}_N + \boldsymbol{\Pi}_M) \cdot \boldsymbol{dS} = \boldsymbol{0} \quad i = (1, 2) \tag{2.8}$$

and torque relative to the cylinder center,

$$\boldsymbol{T} = \int_{S_i} (\boldsymbol{r} - \boldsymbol{r_i}) \times (\boldsymbol{\Pi}_N + \boldsymbol{\Pi}_M) \cdot \boldsymbol{dS} = \boldsymbol{0} \quad i = (1, 2). \tag{2.9}$$

In Eqs. (2.8) and (2.9) $\boldsymbol{\Pi}_N$ and $\boldsymbol{\Pi}_M$ are the Newtonian- and Maxwell-stress tensors

$$\boldsymbol{\Pi}_N = -p\boldsymbol{I} + \mu[\boldsymbol{\nabla u} + (\boldsymbol{\nabla u})^T], \tag{2.10}$$

where $(\ )^T$ denotes the transposition operator, and

$$\boldsymbol{\Pi}_{\boldsymbol{M}} = \boldsymbol{EE} - \tfrac{1}{2}(\boldsymbol{E}\cdot\boldsymbol{E})\boldsymbol{I}, \tag{2.11}$$

respectively.

The contribution of the Maxwell stress to $\boldsymbol{F}$ and $\boldsymbol{T}$ is, in principle, calculated directly from the solution of the above electrochemical problem. Earlier analyses [4,12,13] indicate, however, that dielectrophoresis (DEP) only has a relatively minor effect on the relative motion of ideally polarizable particles under a DC field. We later on return to address this issue in Sec. V. Focusing in the meantime exclusively on ICEP, both the resultant hydrodynamic force and torque need to vanish on the freely suspended particles.

III. ANALYSIS

The present problem is most conveniently described in bipolar cylindrical coordinates $(\alpha,\ \beta)$, defined by the transformation [4,13–15]

$$x = \frac{\sinh\alpha}{\cosh\alpha - \cos\beta}, \quad y = \frac{\sin\beta}{\cosh\alpha - \cos\beta} \tag{3.1}$$

$(-\infty < \alpha < \infty,\ 0 \leqslant \beta < 2\pi)$ from the Cartesian system whose x axis is attached to the LOC with the origin at its mid-point (see Fig. 1). The coordinate lines $\alpha = \text{const}$ are two families of nonintersecting circles centered at $b = (\coth\alpha, 0)$ whose radii are $a = |\text{cosech}\alpha|$; $\beta = const$ describe circular arcs (radii $|\text{cosec}\ \beta|$) leaning on the common chord extending between the pointes $(\pm 1,\ 0)$. Our pair of cylinders thus correspond to $\alpha = \pm\alpha_0$ [$=\cosh^{-1}(b'/a')$] with the dimensional length scale c' and particles radius a' being related through $c' = a'\sinh\alpha_0$.

A. The electrochemical problem

In the bipolar coordinates, Eq. (3.1), the problem governing Φ comprises the equation

$$\frac{\partial^2\Phi}{\partial^2\alpha} + \frac{\partial^2\Phi}{\partial^2\beta} = 0, \tag{3.2}$$

together with the boundary conditions

$$\frac{\partial\Phi}{\partial\alpha} = 0 \quad \text{at } \alpha = \pm\alpha_0 \tag{3.3}$$

and

$$\Phi = -x(\alpha,\beta)\cos\theta - \mathrm{y}(\alpha,\beta)\sin\theta \quad \text{as } \alpha^2 + \beta^2 \to 0. \tag{3.4}$$

The form of the latter and the linearity of the problem suggest the expression of $\Phi(\alpha,\beta)$ as the sum

$$\Phi = \Phi_1(\alpha,\beta)\cos\theta + \Phi_2(\alpha,\beta)\sin\theta \tag{3.5}$$

of the contributions of the components of external field parallel and perpendicular, respectively, to the LOC. These, in turn, are readily obtainable via appropriate domain continuation from the solution [15] presented for the electrophoresis of a dielectric cylinder in the directions perpendicular to a conducting plane or parallel to a dielectric plane as

$$\Phi_1 = -2\sum_{n=1}^{\infty}\frac{e^{-n\alpha_0}}{\cosh n\alpha_0}\sinh n\alpha\cos n\beta - \frac{\sinh\alpha}{\cosh\alpha - \cos\beta} \tag{3.6}$$

and

$$\Phi_2 = -2\sum_{n=1}^{\infty} \frac{e^{-n\alpha_0}}{\sinh n\alpha_0} \cosh n\alpha \sin n\beta - \frac{\sin\beta}{\cosh\alpha - \cos\beta}, \tag{3.7}$$

respectively. For future reference we note that the electric fields corresponding to Φ_1 and Φ_2 have mirror-image symmetries relative to the x and y axes, respectively. Hence Φ_1 is an odd function of α and even with respect to $\beta = \pi$ and conversely for Φ_2. The electric field in bipolar coordinates is obtained via substitution of Eqs. (3.5)–(3.7) in

$$\boldsymbol{E} = -\nabla\Phi = -(\cosh\alpha - \cos\beta)\left(\frac{\partial\Phi}{\partial\alpha}\hat{\boldsymbol{e}}_{\boldsymbol{\alpha}} + \frac{\partial\Phi}{\partial\beta}\hat{\boldsymbol{e}}_{\boldsymbol{\beta}}\right) \tag{3.8}$$

[14] which, in turn, serves to calculate from Eq. (2.11) the Maxwell stress and hence the DEP contribution to particles motion. From Eqs. (3.5)−(3.7) we also obtain the induced zeta potential

$$\zeta = \Phi_w - \Phi(\alpha, \beta) \quad \text{at } \alpha = \pm\alpha_0, \tag{3.9}$$

wherein Φ_w is the uniform potential of the conducting solid and $\Phi(\pm\alpha_0, \beta)$ denotes the local potential at the outer edge of the EDL. The former (Φ_w) is determined from particle-charge conservation. For initially uncharged particles

$$\int_{S_i} q dS = 0 \tag{3.10}$$

[16], wherein q denotes the surface-charge density distribution which (since the diffuse EDL charge completely screens the surface charge) is determined by ζ. Under the assumption [1] of small ζ (relative to the thermal potential) q is proportional to ζ. Combining Eqs. (3.9) and (3.10) we then obtain

$$\Phi_{wi} = \frac{1}{S}\int_{S_i} \Phi dS \quad \text{on} \quad S_i \quad (i = 1, 2). \tag{3.11}$$

From the above symmetry properties, $\Phi_2(\pm\alpha_0, \beta)$ does not contribute to Φ_w. For $\Phi_1(\pm\alpha_0, \beta)$ we recognize that the contribution to Eq. (3.11) of the second term in Eq. (3.6) is simply the x coordinate of the cylinder center, i.e., $\coth\alpha_0$. To evaluate the contribution of the first term in Eq. (3.6) we make use of the integral relation

$$\int_0^{2\pi} \frac{\cos n\beta \, d\beta}{\cosh\alpha_0 - \cos\beta} = \frac{2\pi e^{-n\alpha_0}}{\sinh\alpha_0} \tag{3.12}$$

[17], thereby obtaining

$$\Phi_{wi} = \mp\left(\sum_{n=1}^{\infty} e^{-2n\alpha_0} \tanh n\alpha_0 + \coth\alpha_0\right)\cos\theta \quad \text{at } S_i. \quad (i = 1, 2) \tag{3.13}$$

B. The electro-osmotic flow

Fluid motion is governed by the Stokes-flow problem Eqs. (2.4)–(2.7). The linearity of this problem allows for the superposition of the contributions appearing in Eq. (2.6), i.e., those of the particles rigid-body translational and rotary motions and the electro-osmotic slip $\boldsymbol{u_s}$, respectively. We here focus on the latter which, in turn, drives the fluid as well as particles motion in ICEP.

Making use of $\Phi(\alpha, \beta)$, Eqs. (3.5)−(3.7), at $\alpha = \pm\alpha_0$ together with Φ_w, Eq. (3.13), we obtain the induced zeta potential, Eq. (3.9) which, in conjuction with the electric field, (3.8), then yield for the Helmholtz-Smoluchoski slip velocity, Eq. (2.3),

$$\boldsymbol{u_s} = (\cosh\alpha_0 - \cos\beta)[\mathrm{A}(\alpha_0, \beta)\cos^2\theta \pm \mathrm{B}(\alpha_0, \beta)\sin\theta\cos\theta + \mathrm{C}(\alpha_0, \beta)\sin^2\theta], \text{ at } \alpha = \pm\alpha_0 \tag{3.14}$$

with $\mathrm{A}(\alpha_0, \beta)$, $\mathrm{B}(\alpha_0, \beta)$ and $\mathrm{C}(\alpha_0, \beta)$ as tabulated in the Appendix.

The coefficients A and C are associated with the separate contributions of the external-field components parallel and perpendicular, respectively, to the LOC. Their contributions possess mirror-image symmetry relative to both axes and are of opposite signs representing effects that act towards mutual cancellation at intermediate orientations $\theta(\neq 0, \pi/2)$ of $\boldsymbol{E_0}$ relative to the LOC. The contribution of the coefficient B associated with the interaction of both external-field components, originating from the inherent nonlinearity of $\boldsymbol{u_s}$ in $\boldsymbol{E}$, is antisymmetric with respect to both axes. With diminishing separation distance the absolute value of B is rapidly increasing relative to those of A and C. We thus anticipate the nonlinear interaction effect to become increasingly dominant in particle motion at small separations and intermediate field orientations.

In the present two-dimensional problem at hand fluid-velocity components are derivable from a stream function satisfying the biharmonic equation

$$\nabla^4 \Psi = 0, \tag{3.15}$$

$$u_\alpha = -(\cosh\alpha - \cos\beta)\frac{\partial \Psi}{\partial \beta} \quad \text{and} \quad u_\beta = (\cosh\alpha - \cos\beta)\frac{\partial \Psi}{\partial \alpha}. \tag{3.16}$$

We thus need to determine the biharmonic function $\Psi(\alpha, \beta)$ satisfying the boundary conditions

$$\mathrm{u}_\alpha = 0 \quad \text{and} \quad u_\beta = u_s \quad \text{at } \alpha = \pm\alpha_0, \tag{3.17}$$

which, by Eqs. (3.16), are equivalent to

$$\Psi = \text{const.} \quad \text{at } \alpha = \pm\alpha_0 \tag{3.18}$$

and

$$\frac{\partial \Psi}{\partial \alpha} = \mathrm{A}(\alpha_0, \beta)\cos^2\theta \pm \mathrm{B}(\alpha_0, \beta)\sin\theta\cos\theta + \mathrm{C}(\alpha_0, \beta)\sin^2\theta \tag{3.19}$$

at $\alpha = \pm\alpha_0$, respectively, as well as the far-field condition, Eq. (2.7). Representing Ψ as the sum

$$\Psi = \Psi_1 + \Psi_2$$

of Ψ_1 associated with the contributions to $\boldsymbol{u_s}$ of A and C and Ψ_2 similarly associated with the coefficient B then, by the above symmetry properties

$$\Psi_1(\alpha, 2\pi - \beta) = \Psi_1(-\alpha, \beta) = -\Psi_1(\alpha, \beta) \tag{3.20}$$

and

$$\Psi_2(\alpha, 2\pi - \beta) = \Psi_2(-\alpha, \beta) = \Psi_2(\alpha, \beta). \tag{3.21}$$

Both Ψ_1 and Ψ_2 may be assigned arbitrary constant values on one of the cylinders. In view of the above symmetry relations, we may, without loss of generality, impose

$$\Psi_1 = \Psi_2 = 0 \quad \text{at} \quad \alpha = \pm\alpha_0. \tag{3.22}$$

Splitting the general separation-of-variables solution of Eq. (3.15) in bipolar coordinates [18,19] into its symmetric and antisymmetric parts and applying Eq. (3.22), we obtain

$$(\cosh\alpha - \cos\beta)\Psi_1 = C_1\left(\sinh 2\alpha - \frac{\sinh 2\alpha_0}{\alpha_0}\alpha\right)\sin\beta + \sum_{k=2}^{\infty}\left\{C_k\left[\sinh(k+1)\alpha - \frac{\sinh(k+1)\alpha_0}{\sinh(k-1)\alpha_0}\sinh(k-1)\alpha\right]\sin k\beta\right\} \tag{3.23}$$

and

$$(\cosh\alpha-\cos\beta)\Psi_2 = A_0\left(\cosh\alpha-\frac{\coth\alpha_0}{\alpha_0}\alpha\sinh\alpha\right)+A_1(\cosh 2\alpha-\cosh 2\alpha_0)\cos\beta + \sum_{k=2}^{\infty}\left\{\left[A_k\cosh(k+1)\alpha-\frac{\cosh(k+1)\alpha_0}{\cosh(k-1)\alpha_0}\cosh(k-1)\alpha\right]\cos k\beta\right\}. \tag{3.24}$$

The coefficients $C_k(k=1,2,\ldots)$ and $A_k(k=0,1,2,\ldots)$ are finally obtained from Eqs. (3.14) and (3.19)

$$C_1\left(2\cosh 2\alpha-\frac{\sinh 2\alpha_0}{\alpha_0}\right)\sin\beta+\sum_{k=2}^{\infty}\{C_k[(k+1)\cosh(k+1)\alpha_0 - (k-1)\sinh(k+1)\alpha_0\coth(k-1)\alpha_0]\sin k\beta\} = (\cosh\alpha_0-\cos\beta)[\mathrm{A}(\alpha_0,\beta)\cos^2\theta+\mathrm{C}(\alpha_0,\beta)\sin^2\theta] \tag{3.25}$$

and

$$A_0\left(\sinh\alpha_0-\frac{\cosh\alpha_0}{\alpha_0}-\coth\alpha_0\cosh\alpha_0\right)+A_1(2\sinh 2\alpha_0)\cos\beta + \sum_{k=2}^{\infty}\{A_k[(k+1)\sinh(k+1)\alpha_0-(k-1)\cosh(k+1)\alpha_0\tanh(k-1)\alpha_0]\cos k\beta\} = (\cosh\alpha_0-\cos\beta)B(\alpha_0,\beta)\sin\theta\cos\theta, \tag{3.26}$$

for the antisymmetric and symmetric parts, respectively. With $\mathrm{A}(\alpha_0,\beta)$, $\mathrm{B}(\alpha_0,\beta)$ and $\mathrm{C}(\alpha_0,\beta)$ as tabulated in the Appendix, the various coefficients are determined by making use of the orthogonality of the circular functions of β in a straightforward but rather tedious calculation omitted here.

The ICEO flow fields corresponding to the stream function thus obtained are depicted in Fig. 2. The solid lines represent the streamline pattern where the sense of fluid motion is indicated by the arrows and fluid speed by the color code. The effect of the orientation of the external field relative to the LOC is illustrated for a pair of cylinders whose centers are four radii apart (i.e., $\alpha_0=\cosh^{-1}2$) at the indicated values of θ. Evidently, unlike linear electrokinetic problems, the asymmetric streamline patterns for $\theta=\pi/6$ and $\pi/3$ cannot be constructed via superposition of the cases $\theta=0$ and $\pi/2$.

Toward subsequent calculation of the freely suspended particles motion we consider the far-field variation of fluid velocity in the above ICEO flow. As is often the case with 2D (planar) Stokes flows, the electro-osmotic velocity field is uniquely determined in the above calculation without invoking the far-field condition Eq. (2.7). Substituting Eqs. (3.23) and (3.24) in Eq. (3.16) we find that the velocity field associated with Ψ_1 trivially satisfies far-field attenuation, whereas the contribution of Ψ_2 becomes

$$(u_{2\alpha},u_{2\beta})=\frac{H(\alpha_0)\cos\theta\sin\theta}{\cosh\alpha-\cos\beta}(\sin\beta,\ -\sinh\alpha)+O(r^{-1}), \tag{3.27}$$

where

$$H_0(\alpha_0)=A_0+A_1(1-\cosh 2\alpha_0)+\sum_{k=2}^{\infty}A_k\left[1-\frac{\cosh(k+1)\alpha_0}{\cosh(k-1)\alpha_0}\right], \tag{3.28}$$

which diverges as $\alpha^2+\beta^2\to 0$. By use of the relations

$$\hat{\boldsymbol{e}}_{\boldsymbol{x}}=\frac{1}{\cosh\alpha-\cos\beta}[-(\cosh\alpha\cos\beta-1)\hat{\boldsymbol{e}}_{\boldsymbol{\alpha}}-\sinh\alpha\sin\beta\hat{\boldsymbol{e}}_{\boldsymbol{\beta}}] \tag{3.29a}$$

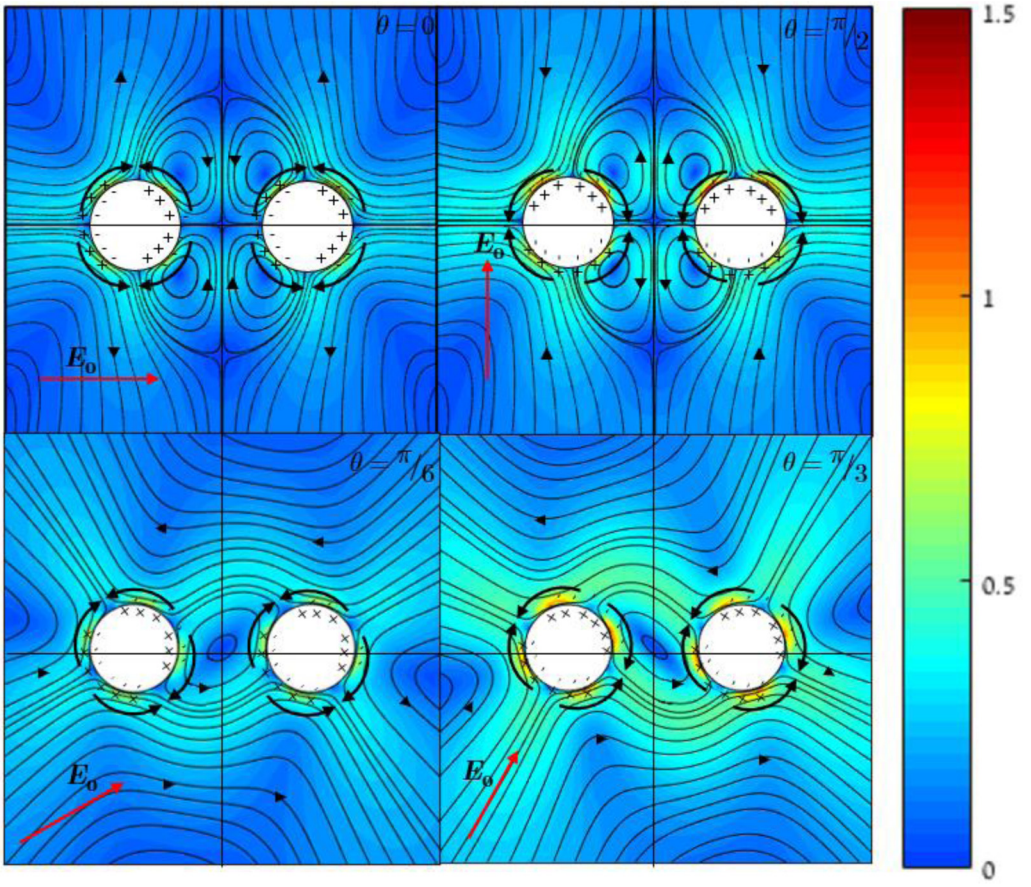

FIG. 2. Electroosmotic streamline patterns around a pair of identical conducting cylinders whose centers are four radii apart. The red arrows mark the directions of the external field $\theta = 0, \pi/2, \pi/6$, and $\pi/3$ relative the line of centers.

and

$$\hat{\boldsymbol{e}}_y = \frac{1}{\cosh\alpha - \cos\beta}[-\sinh\alpha \sin\beta \hat{\boldsymbol{e}}_{\boldsymbol{\alpha}} + (\cosh\alpha\cos\beta - 1)\hat{\boldsymbol{e}}_{\boldsymbol{\beta}}] \tag{3.29b}$$

between the unit vectors $(\hat{\boldsymbol{e}}_{\boldsymbol{x}},\ \hat{\boldsymbol{e}}_{\boldsymbol{y}})$ of the Cartesian system and $(\hat{\boldsymbol{e}}_{\boldsymbol{\alpha}}, \hat{\boldsymbol{e}}_{\boldsymbol{\beta}})$ of the bipolar system [14] one obtains for the leading-order Cartesian components of $\boldsymbol{u}_2$

$$(u_{2x}, u_{2y}) = H(\alpha_0)\cos\theta \sin\theta(y,\ -x), \quad \text{as } x^2 + y^2 \to \infty \tag{3.30}$$

representing a rigid-body rotation. To compensate for this contribution of the induced electro-osmotic flow and satisfy the attenuation condition of the far-field fluid velocity, the motion of the freely suspended cylinder pair will include an antisymmetric mode consisting of a combination of equal angular velocities and opposing equal-magnitude transverse translational velocities perpendicular to the line of centers [20] as schematically depicted in Fig. 3(b). By the symmetry of the corresponding induced electro-osmotic flow, the contribution associated with Ψ_1 will give rise to a perfectly symmetric translational motion of the pair of cylinders along their line of centers [Fig. 3(a)].

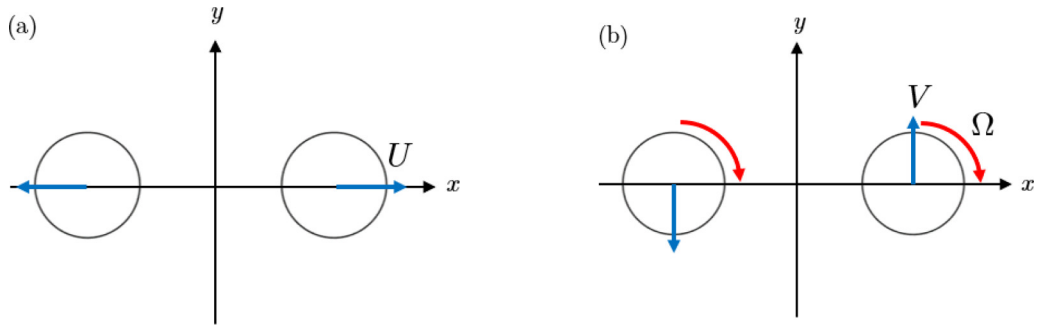

FIG. 3. Schematic representation of the translational and angular velocities of the cylinders associated with Ψ_1 (a) and Ψ_2 (b). Similarly to Ref. [20], in part (b) the transverse velocities of the cylinders $\boldsymbol{\alpha} = \pm\boldsymbol{\alpha}_0$ are depicted as $\pm\hat{\boldsymbol{e}}_y\, V$, $(V > 0)$, respectively, with their common angular velocity $\boldsymbol{\Omega} = \hat{\boldsymbol{e}}_z\, \Omega$, $(\Omega < 0)$, and $\hat{\boldsymbol{e}}_z$ a unit vector in the positive z direction [cf. Eq. (4.9)].

IV. RELATIVE ICEP PARTICLE MOTION

Actual calculation of the velocities of the freely suspended particles, avoiding the need for an explicit calculation of the velocity and stress fields in the present problem, is conveniently carried out via application of the Lorentz reciprocal theorem

$$\int_S \boldsymbol{dS} \cdot \boldsymbol{\Pi}_2 \cdot \boldsymbol{u}_1' = \int_S \boldsymbol{dS} \cdot \boldsymbol{\Pi}_1 \cdot \boldsymbol{u}_2, \tag{4.1}$$

where $\boldsymbol{\Pi}_i$ and $\boldsymbol{u}_i$ $(i = 1, 2)$ are pairs of stress-tensor and velocity-vector fields, respectively, satisfying the creeping-flow equations within the same domain. The relation holds for an arbitrary closed surface S bounding any fluid volume [21]. The above relationship is particularly useful provided that a comparison solution of the continuity and Stokes equations within the same fluid domain is available, which is indeed the case here (cf. Ref. [20]).

In the present problem S comprises the union of S_1 and S_2, effectively coinciding with the particles surfaces together with S_∞, an arbitrary closed surface lying in the far field as schematically depicted in Fig. 4. Furthermore, the pairs $(\boldsymbol{u}_i, \boldsymbol{\Pi}_i)$ are selected so that S_∞ has a vanishing contribution.

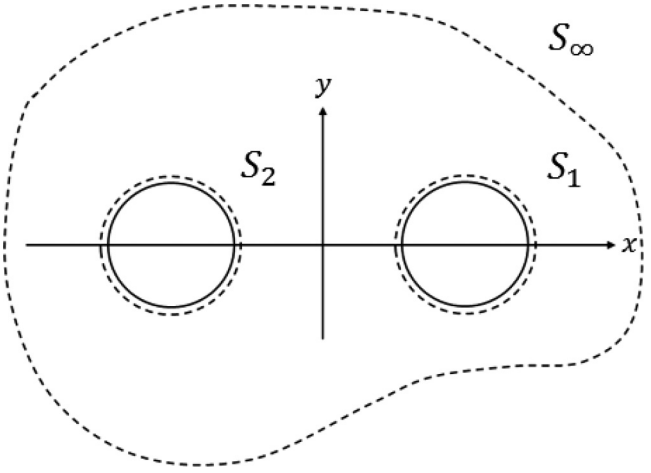

FIG. 4. The surface $\boldsymbol{S}$ bounding the fluid domain.

As indicated in the above electro-osmotic-flow analysis, the relative ICEP motion is analyzed via superposition of the contributions of Ψ_1, giving rise to a perfectly symmetric translational motion of the pair of cylinders along their line of centers [Fig. 3(a)], and Ψ_2 inducing an antisymmetric motion of the cylinders consisting of a combination of equal angular velocities and opposing equal-magnitude translational velocities perpendicular to the line of centers [as in Fig. 3(b)].

A. Symmetric motion

The reciprocal theorem is here implemented via comparison of the symmetric part of the present problem (denoted by subscript 1), i.e., the motion generated by the slip velocity

$$\boldsymbol{u}_{s_1} = \hat{\boldsymbol{e}}_{\boldsymbol{\beta}}(\cosh\alpha_0 - \cos\beta)[\mathrm{A}(\alpha_0,\beta)\cos^2\theta + \mathrm{C}(\alpha_0,\beta)\sin^2\theta], \tag{4.2}$$

giving rise to a perfectly symmetric translational motion of the pair of cylinders along their LOC with a velocity $\hat{\boldsymbol{e}}_{\boldsymbol{x}}U_1$ (yet to be determined) with the reference problem (denoted by subscript 2) of a pair of cylinders symmetrically translating along their line of centers with an arbitrary speed U_2. The far-field decay condition is here trivially satisfied for both problems [20] and thus the contributions of the integrals on S_∞ indeed vanish. Substitution in Eq. (4.1) and use of the symmetry properties of the problem provides

$$\int_{\alpha_0} \boldsymbol{dS}\cdot\boldsymbol{\Pi}_2\cdot\left(\hat{\boldsymbol{i}}U_1 + \boldsymbol{u}_{s_1}\right) = \int_{\alpha_0} \boldsymbol{dS}\cdot\boldsymbol{\Pi}_1\cdot\hat{\boldsymbol{i}}U_2, \tag{4.3}$$

which, after integration, yields

$$F_{x2}U_1 - \int_0^{2\pi} \frac{\Pi_{\alpha\beta 2}u_{s_1}d\beta}{\cosh\alpha_0 - \cos\beta} = F_{x1}U_2, \tag{4.4}$$

wherein F_{x1} and F_{x2} denote the resultant hydrodynamic axial forces in the present and comparison problems, respectively. Furthermore, $\Pi_{\alpha\beta 2}$ and F_{x2} are linear in U_2 [20]

$$F_{x2} = -\frac{8\pi U_2}{2\alpha_0 - \tanh 2\alpha_0}, \tag{4.5}$$

and

$$\Pi_{\alpha\beta 2} = \frac{4U_2\sinh 2\alpha_0\sin\beta}{\sinh 2\alpha_0 - 2\alpha_0\cosh 2\alpha_0}(\cosh\alpha_0 - \cos\beta). \tag{4.6}$$

Neglecting at this stage the DEP force, the resultant viscous force on the freely suspended particles vanishes as well, $F_{x1} = 0$. Substitution of Eqs. (4.5) and (4.6) in Eq. (4.4) then yields

$$U_1 = -\frac{1}{2\pi}\tanh 2\alpha_0\int_0^{2\pi} u_{s_1}(\alpha_0,\beta)\sin\beta d\beta. \tag{4.7}$$

B. Anti-symmetric motion

The reciprocal theorem is here implemented via comparison of the fluid and particle motion associated with the slip velocity

$$\boldsymbol{u}_{s_1} = \pm\hat{\boldsymbol{e}}_{\boldsymbol{\beta}}(\cosh\alpha_0 - \cos\beta)\mathrm{B}(\alpha_0,\beta)\sin\theta\cos\theta, \tag{4.8}$$

giving rise to the antisymmetric mode of motion consisting of a combination of (as yet unknown) equal angular velocities $\boldsymbol{\Omega} = \hat{\boldsymbol{e}}_z\,\Omega_1$ and opposing equal-magnitude translational velocities $\pm\hat{\boldsymbol{e}}_y\,V_1$ perpendicular to the LOC [cf. Fig. 3(b)] and the corresponding reference problem of a pair of cylinders having equal angular velocities $\boldsymbol{\Omega} = \hat{\boldsymbol{e}}_z\,\Omega_2$ and opposing equal-magnitude translational

velocities perpendicular to the line of centers $\pm\hat{\boldsymbol{e}}_{\boldsymbol{y}}\, V_2$, satisfying, in turn, no slip and the relation [20]

$$V_2 = -\frac{\alpha}{\sinh^2\alpha}\Omega_2, \tag{4.9}$$

for $\alpha = \pm\alpha_0$ [where similarly to Fig. 3(b), $\Omega_2 < 0$], ensuring far-field decay of the reference velocity field. As mentioned above, this requirement is not trivially satisfied in the present problem and is addressed next. Pending this, we substitute the above in Eq. (4.1) while omitting the contribution on S_∞ to obtain

$$\int_{\alpha_0} \boldsymbol{dS}\cdot\boldsymbol{\Pi}_2\cdot\left(\hat{\boldsymbol{e}}_{\boldsymbol{y}}\, V_1 + \hat{\boldsymbol{e}}_z\,\Omega_1\times\,(\boldsymbol{r}-\boldsymbol{r_i}) + \boldsymbol{u}_{s_1}\right) = \int_{\alpha_0}\boldsymbol{dS}\cdot\boldsymbol{\Pi}_1\cdot[\hat{\boldsymbol{e}}_{\boldsymbol{y}}\, V_2 + \hat{\boldsymbol{e}}_z\,\Omega_2\times(\boldsymbol{r}-\boldsymbol{r_i})]. \tag{4.10}$$

Carrying out the integration yields

$$F_{y_2}V_1 + T_2\Omega_1 - \int_0^{2\pi}\frac{\Pi_{\alpha\beta 2}u_{s_1}d\beta}{\cosh\alpha_0-\cos\beta} = F_{y_1}V_2 + T_1\Omega_2. \tag{4.11}$$

Similarly to the above, in view of the required vanishing of the resultant force and torque on the freely suspended particles, in the absence of DEP the hydrodynamic force and torque both vanish, $F_{y_1},\ T_1 = 0$, resulting in

$$F_{y_2}V_1 + T_2\Omega_1 = \int_0^{2\pi}\frac{\Pi_{\alpha\beta 2}u_{s_1}d\beta}{\cosh\alpha_0-\cos\beta}. \tag{4.12}$$

Use of the relations [20]

$$F_{y_2} = \frac{4\pi\Omega_2}{\sinh^2\alpha_0},\quad T_2 = -\frac{4\pi\Omega_2\cosh\alpha_0}{\sinh^3\alpha_0},\quad \Pi_{\alpha\beta 2} = \frac{2(\cosh\alpha_0-\cos\beta)\Omega_2\cosh\alpha_0}{\sinh^2\alpha_0},$$

then yields a first equation for V_1 and Ω_1

$$V_1 - \Omega_1\coth\alpha_0 = -\frac{\cosh\alpha_0}{2\pi}\int_0^{2\pi}u_{s_1}(\alpha_0,\beta)d\beta. \tag{4.13}$$

A second equation results from imposing the attenuation condition (2.7). The far-field fluid velocity is represented via the superposition of the contributions of translation with the velocities $\pm\hat{\boldsymbol{e}}_{\boldsymbol{y}}\, V_1$, rotation of the particles with the equal angular velocity $\hat{\boldsymbol{e}}_z\,\Omega_1$, and the electro-osmotic contribution of $\boldsymbol{u}_{s_1}$. By the definition, Eq. (3.1), of the bipolar coordinates

$$r^2 = x^2+y^2 = \frac{\cosh\alpha+\cos\beta}{\cosh\alpha-\cos\beta} \sim \frac{4}{\alpha^2+\beta^2}[1+O(\alpha^2,\beta^2)],$$

$r \gg 1$ corresponds to $\alpha,\beta \ll 1$, namely $\alpha,\beta \sim O(r^{-1})$. Thus, the former pair of contributions to the far field are [20]

$$\boldsymbol{u}_{\boldsymbol{V_1}} \sim \frac{V_1\sinh^2\alpha_0}{\alpha_0+\sinh\alpha_0\cosh\alpha_0}(-y,x) + O(r^{-1})$$

and

$$\boldsymbol{u}_{\boldsymbol{\Omega_1}} \sim \frac{\Omega_1\alpha_0}{\alpha_0+\sinh\alpha_0\cosh\alpha_0}(-y,x) + O(r^{-1}),$$

while $\boldsymbol{u_{EO}}$, the corresponding electro-osmotic contribution, has been obtained in Eqs. (3.28) and (3.30). The attenuation condition thus yields the required second equation for V_1 and Ω_1, namely

$$V_1\sinh^2\alpha_0 + \Omega_1\alpha_0 = \tfrac{1}{2}H_0(\alpha_0)(2\alpha_0+\sinh 2\alpha_0)\sin\theta\cos\theta. \tag{4.14}$$

With a view to subsequent analysis of particle trajectories, the original length scale c' which, for constant particle radius a' is varying with separation, is replaced by the latter. Thus, the value

of α corresponding to the particle pair is now varying with the center separation, $r = \cosh\alpha$. Accordingly, instead of α_0 we henceforth use α (which, by the symmetry properties of the various modes of relative motion is, similarly to α_0, considered positive). Rescaling velocities with the particle radius a' as a characteristic length we have

$$\frac{\varepsilon' E_0'^2 c'}{\mu'}(U,\ V) \rightarrow \frac{\varepsilon' E_0'^2 a'}{\mu'}(\bar{U}, \bar{V}) \tag{4.15a}$$

with, since $c' = a' \sinh\alpha$,

$$(\bar{U},\ \bar{V}) = (U,\ V)\sinh\alpha. \tag{4.15b}$$

Thus,

$$\bar{U}(\alpha, \theta) = \bar{A}(\alpha)\cos^2\theta + \bar{C}(\alpha)\sin^2\theta, \tag{4.16a}$$

where, by substituting Eq. (4.2) in Eq. (4.7), we obtain

$$(\bar{A}(\alpha), \bar{C}(\alpha)) = -\frac{\tanh 2\alpha \sinh\alpha}{2\pi}\int_0^{2\pi}[A(\alpha, \beta), C(\alpha, \beta)](\cosh\alpha - \cos\beta)\sin\beta d\beta \tag{4.16b}$$

with $A(\alpha, \beta)$ and $C(\alpha, \beta)$ as given in Eqs. (A1) and (A3). Similarly to the above we obtain from Eqs. (4.8), (4.13), and (4.14)

$$\bar{V}_1 = \sinh\alpha V_1 = -\bar{B}(\alpha)\cos\theta\sin\theta, \tag{4.17a}$$

where

$$\bar{B} = \left[H_0(\alpha)\cosh\alpha + \frac{\alpha\sinh\alpha\cosh\alpha}{2\pi\left(\alpha + \frac{1}{2}\sinh 2\alpha\right)}\int_0^{2\pi} B(\alpha, \beta)(\cosh\alpha - \cos\beta)d\beta\right] \tag{4.17b}$$

with $H_0(\alpha)$ and $B(\alpha, \beta)$ as given in Eqs. (3.28) and (A2), respectively.

C. Particle paths

Particle-center paths are described relative to a stationary frame (X, Y) with its X axis aligned with the (constant) direction of the uniform external field and its origin, as before, at the stationary LOC midpoint. Denote by θ_1 the instantaneous orientation of the LOC (the X axis in Fig. 1) relative to the new X axis. The instantaneous radial- and tangential-velocity components (along the LOC and perpendicular thereto, respectively) are readily obtained from the above results via the substitution $\theta = -\theta_1$ (cf. Fig. 1). Particle-center trajectories are thus calculated via integration of the quasistationary kinematic equations of motion

$$\dot{r} = \bar{U}(\alpha, \theta_1) = \bar{A}(\alpha)\cos^2\theta_1 + \bar{C}(\alpha)\sin^2\theta_1 \tag{4.18}$$

and

$$r\dot{\theta}_1 = \bar{V}(\alpha, \theta_1) = \bar{B}(\alpha)\cos\theta_1\sin\theta_1, \tag{4.19}$$

based on the instantaneous geometric configuration ($r = \cosh\alpha, \theta_1$; as mentioned above, α is now varying with particle location).

Appearing in the above are the coefficients $\bar{A} < 0$ ($\bar{C} > 0$) associated with the attractive (repulsive) effects of the external-field components parallel (perpendicular) to LOC, respectively, and the coefficient $\bar{B}$ representing the interaction effect of both external-field components resulting in LOC rotation. Figure 5 presents the variation of these coefficients with the distance r of the particle center from the LOC midpoint (i.e., half the center-separation distance). With diminishing particles separation $\bar{A}$ is vanishing while $\bar{C}$ is approaching a finite limit. These reflect the difference between the weak- and strong- local fields within the narrow gap for nearly touching particles under an external field parallel or perpendicular to the line-of-centers, respectively. We further

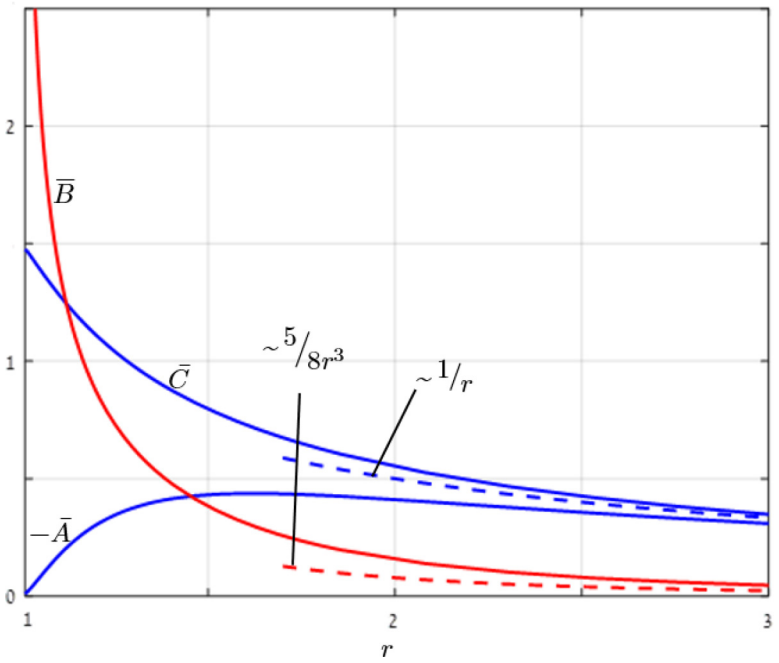

FIG. 5. Variation with the distance r (scaled by particle radius) of the coefficients $\bar{A}, \bar{C}$, and $\bar{B}$ and their corresponding asymptotes (solid and dashed lines, respectively).

note that, at small separations, $\bar{B}$ becomes substantially larger than both $\bar{C}$ and $|\bar{A}|$. Thus, at these relatively small values of r and intermediate LOC orientations, $\tan^{-1}(|\bar{A}/\bar{B}|) \lesssim \theta_1 \lesssim \tan^{-1}(|\bar{B}/\bar{C}|)$, we anticipate relative particle-pair motion to be dominated by LOC rotations associated with the nonlinear interaction of both external-field components.

With increasing r, the magnitudes of $\bar{A}$ and $\bar{C}$ are both diminishing like $\sim 1/r$, becoming nearly equal for $r \gtrsim 3$; the coefficient $\bar{B}$ is diminishing much more rapidly, like $\sim(5/8)\, r^{-3}$ as presented by the corresponding (dashed) asymptotes. At large r we therefore anticipate a slow, nearly radial (along LOC), inwards or outwards motion according as $\theta_1 < \pi/4$ or $\theta_1 > \pi/4$, respectively; for $\theta_1 \approx \pi/4$ where the effects associated with $\bar{A}$ and $\bar{C}$ are mutually canceling, the small positive $\bar{B}$ results in a slow counterclockwise (clockwise) LOC rotation for the particle pairs residing in the first and third (second and fourth) quadrants, respectively.

The close agreement between the coefficients $\bar{A}$, $\bar{C}$ and $\bar{B}$ and their respective leading-order asymptotic approximations, as observed in Fig. 5 already at $r \gtrsim 3$, suggests an approximate analytic description of moderately remote particle-center trajectories. To this end we replace in Eqs. (4.18) and (4.19) the coefficients $\bar{A}$, $\bar{C}$, and $\bar{B}$ by their asymptotic counterparts thereby obtaining the simplified kinematic equations of motion

$$\dot{r} \sim r^{-1} \cos(2\theta_1) \quad \text{and} \quad r\dot{\theta}_1 \sim (5/8)\, r^{-3} \sin(2\theta_1) \tag{4.20}$$

indicating minima $r = r_{\min}$ at $\theta_1 = \pi/4$. Integration of Eqs. (4.20) readily yields a single-parameter family of particle-center paths

$$\sin(2\theta_1) = \exp\left[(5/16)\left(1/r^2 - 1/r_{\min}^2\right)\right] \tag{4.21}$$

symmetric about $\theta_1 = \pi/4$.

Figure 6 presents the cylinder-pair motion under a uniform DC field parallel to the X axis as obtained via integration of the above kinematic equations of motion. This has been carried out for $r \geqslant 1.01$ inasmuch as for microparticles at smaller separations the very assumption of thin EDL may

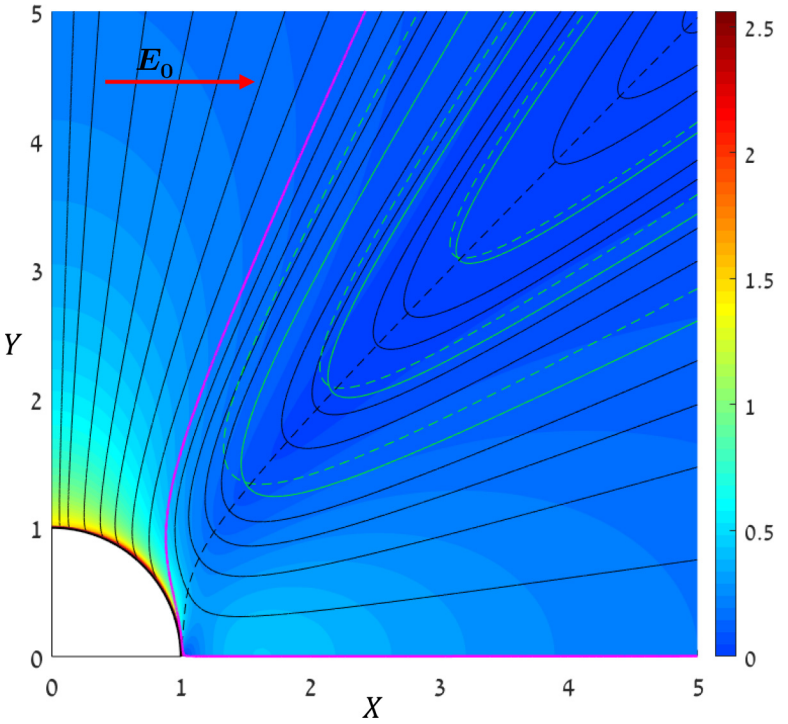

FIG. 6. The cylinder– pair relative motion: Paths (solid lines) and local speed (color code) of particle-center motion relative to (stationary) midpoint of line-of-centers under a uniform DC field parallel to X axis. Coordinates are scaled by particle radius (hence white quarter unit circle inaccessible to particle center). Light-green curves present pairs of exact- and (moderately large separation) approximate-trajectories corresponding to common values of $r_{\min}$ (= 2, 3, and 4.4, respectively).

not apply within the narrow gap. Point symmetry relative to the origin (the stationary midpoint of the LOC) together with the mirror-image symmetry relative to both axes allows us to limit description to the first quadrant of the (X, Y) plane. With coordinates now scaled by particle radius, the white quarter unit circle marks the domain inaccessible to particle center. The solid lines describe particle-center trajectories with the local speed represented by the color code, both obtained from Eqs. (4.18) and (4.19). The light-green curves present pairs of exact (solid) and approximate (dashed, obtained from Eqs. (4.20) for moderately large separation) trajectories corresponding to common values of $r_{\min}$ (= 2, 3, and 4.4, respectively); the purple line which (on the scale of the figure) initially appears to nearly coincide with the X axis, describes the path for which $r_{\min} = 1.01$ (with any path starting nearer to the X axis reaching excluded separations $r < 1.01$). As such, the purple curve delimits the domain of entire trajectories entering from the right (at $X = 5$, $Y \geqslant 0.003$) and leaving at the top of the figure ($X \geqslant 2.43$, $Y = 5$). Accordingly, the paths to the left of the purple line result from integration of Eqs. (4.18) and (4.19) starting at points $r = 1.01$ just above the excluded domain.

The general trends observed agree with the above qualitative predictions based on the variation with particles separation of $\bar{A}, \bar{C}$, and $\bar{B}$. The dashed curve marks the locus of points of zero radial velocity, thus dividing the plane into subdomains of inward and outward motion (below and above this line, respectively). Since $|\bar{A}|$ is vanishing as $r \to 1$ this curve emanates from a small $\theta_1 (\approx 4.5^\circ$ for $r = 1.01)$ and with increasing r, in agreement with the above observed near equality of $\bar{C}$ and $|\bar{A}|$, asymptotically approaches the ray $\theta_1 = \pi/4$. Together with the rapid decrease of $\bar{B}$, for moderate (and larger) r, away from this line, the motion is indeed essentially radial. In the vicinity of this line, pair motion is dominated by the LOC rotation associated with the nonlinear

interaction effect, which becomes more prominent with diminishing separation. Since $\bar{B} > 0$ for all r, the nonlinear interaction between both external-field components gives rise to a counterclockwise LOC rotation for all particles at $\theta_1 \neq 0,\ \pi/2$. Thus, within the present calculation, practically all particles are eventually moving away from each other in the general direction perpendicular to the external field. Particles which are initially located under the dashed curve experience transient pairing events qualitatively similar to those described by Saintillan [7] in the corresponding problem of the relative ICEP motion of spherical-particle pairs.

The approximate moderately far trajectories (4.21) are symmetric relative to $\theta_1 = \pi/4$ and, with increasing $r_{\min}$, appear confined to a narrower sector. For $r_{\min} = 2$ the dashed curve only provides a qualitative approximation to the corresponding exact path, owing to asymmetry of the latter associated with the inequality $|\bar{A}| < \bar{C}$, i.e., outward radial motion being generally faster than the corresponding inward one. This asymmetry is all the more noticeable the closer the path starting point is to the X axis. The ensuing path then attains a smaller $r_{\min}$ and the particle stays longer where the difference between $\bar{C}$ and $|\bar{A}|$ is large while $\bar{B}$ being larger than both with the relative motion thus dominated by (counterclockwise) LOC rotation. At $r_{\min} = 2$, $\bar{C}$ is still nearly 40% larger than $|\bar{A}|$. With increasing $r_{\min}$ the difference between $\bar{C}$ and $|\bar{A}|$ is decreasing hence the trajectory asymmetry and associated error in the approximate path are visibly diminishing.

As mentioned above, within the present calculation the trajectories at the left part of the figure strictly describe particle-center motion emanating at $r = 1.01$, just above the inaccessible domain, i.e. when both particles are nearly in contact. An interesting issue regards the origin of these particles. While no conclusive answer is provided within the present model, we may gain some qualitative insight focusing on the purple path following its passage through $r_{\min} = 1.01$ where $|\bar{A}|/\bar{C} \approx 6 \times 10^{-3}$ and $\bar{C}/\bar{B} \approx 0.3$. Beyond this point $\bar{U}/\bar{V} < \bar{C}(r)/\bar{B}(r)\tan\theta_1$. Thus the particle-center follows a nearly circular arc (with the particle pair thus rotating like a rigid dumbbell) until $\tan\theta_1$ increases sufficiently to allow for a significant radial motion, which only becomes visible for $\theta_1 \approx 16^\circ$. Extrapolating to still smaller $r_{\min}$ (< 1.01), $\bar{C}/\bar{B}$ becomes smaller with the corresponding paths following a longer nearly circular arc before emerging above the excluded domain at a larger θ_1. Thus, these paths may represent the later phase of relative particle-center motion for pairs starting with their LOC closer to field direction than the corresponding initial orientation for the purple path. Evidently, this rather *ad hoc* extrapolation cannot serve to relate the paths at the left of the figure to their earlier-phase counterparts.

Finally, in marked contrast to the present results, the finite-volume simulations of Kang [12] predict that ICEP makes both particles follow spiral trajectories converging on stationary points (at a finite separation from each other). This mode of motion is attributed to the presence of the square-cavity walls. Indeed, the above calculation of the antisymmetric mode of particle-pair motion (V, Ω) is intimately related to the attenuation condition, Eq. (4.14). Apparently, imposing instead no-slip at a $finite$ distance, on the cavity walls, can significantly modify the resulting pair motion.

V. DEP EFFECT ON THE RELATIVE (DIP) PARTICLE MOTION

Making use of the electric field, Eq. (3.8), obtained from the solution of the electrochemical problem, Eqs. (3.5)–(3.7), one readily obtains $\mathbf{\Pi}_{\boldsymbol{M}}$, Eq. (2.11), and the resultant electric force $\boldsymbol{F^M} = \hat{\boldsymbol{e}}_{\boldsymbol{x}} F_x^M + \hat{\boldsymbol{e}}_{\boldsymbol{y}} F_y^M$ and torque $\boldsymbol{T^M} = \hat{\boldsymbol{e}}_{\boldsymbol{z}}\, T^M$ from the corresponding parts of Eqs. (2.8) and (2.9), respectively. By the required vanishing of the resultant force and torque on the freely suspended particles $\boldsymbol{F^M}$ and $\boldsymbol{T^M}$ would then show up in the equations resulting from application of the reciprocal theorem. We note that, by the homogeneous Neumann condition, Eq. (2.1), the electric field is tangent to the particle surface and the associated local traction vector is normal thereto, i.e., in the radial direction, hence no electric torque is generated on the circular cylindrical particles, $T^M = 0$. By use of the transformation of the unit vectors, Eqs. (3.29a) and (3.29b), the components

of $\boldsymbol{F^M}$ obtained from Eq. (2.8) are

$$F_x^M = \pm \int_0^{2\pi} \frac{1}{(\cosh\alpha - \cos\beta)^2}\left[\frac{1}{2}(1-\cosh\alpha\cos\beta)(E_\beta E_\beta - E_\alpha E_\alpha) + E_\alpha E_\beta \sinh\alpha \sin\beta\right] d\beta, \tag{5.1}$$

and

$$F_y^M = \pm \int_0^{2\pi} \frac{1}{(\cosh\alpha - \cos\beta)^2}\left[\frac{1}{2}\sinh\alpha\sin\beta(E_\alpha E_\alpha - E_\beta E_\beta) + E_\alpha E_\beta(1-\cosh\alpha\cos\beta)\right] d\beta, \tag{5.2}$$

at $\alpha = \pm\alpha_0$, respectively. From the symmetry properties of the electric field on the surface of the cylinders, we obtain

$$F_x^M = \bar{A}^M(\alpha)\cos^2\theta + \bar{C}^M(\alpha)\sin^2\theta \quad \text{and} \quad F_y^M = \pm\bar{B}^M(\alpha)\sin\theta\cos\theta. \tag{5.3}$$

Actual calculation of $\bar{A}^M$, $\bar{C}^M$, and $\bar{B}^M$ is straightforward but tedious resulting in cumbersome expressions, which are therefore omitted here.

Substituting $F_{x1} = -F_x^M$ on the RHS of Eq. (4.4) while making use of Eq. (4.5) we obtain the relative DEP contributions to the rescaled [with respect to a', cf. Eq. (4.15)] particle velocity along LOC represented by the ratios

$$(R_{\bar{A}}, R_{\bar{C}}) = \left(\frac{1}{8\pi}\right)(2\alpha - \tanh 2\alpha)\left[\frac{\bar{A}^M(\alpha)}{\bar{A}(\alpha)}, \frac{\bar{C}^M(\alpha)}{\bar{C}(\alpha)}\right]. \tag{5.4}$$

For the antisymmetric mode of motion we substitute on the RHS of Eq. (4.11) $F_{y_1} = -F_y^M$ and $T_1 = 0$. The relative DEP contribution to the rescaled transverse velocities resulting from the thus modified Eq. (4.11) together with Eq. (4.14) is

$$R_{\bar{B}} = \frac{\alpha^2 \sinh 2\alpha}{2\pi(2\alpha + \sinh 2\alpha)}\left[\bar{F}_y^M(\alpha)/\bar{B}(\alpha)\right]. \tag{5.5}$$

For future reference we note that both $\bar{A}(\alpha)$ and $\bar{A}^M(\alpha)$ represent attractive forces, being both positive (negative) for $\alpha > 0$ (<0). The opposite signs apply to the pair $\bar{C}(\alpha)$ and $\bar{C}^M(\alpha)$ both representing, in turn, repulsive forces. In contrast $\bar{B}$ and $\bar{F}_y^M$ have opposite signs. Thus, ICEP acts to rotate LOC to an orientation perpendicular to $\boldsymbol{E}_0$ whereas DEP acts to align it with the external field. Figure 7 presents the variation with r of $R_{\bar{A}}$, $R_{\bar{C}}$, and $R_{\bar{B}}$. The peak values of the former ratios are slightly over 3%. Because of this small relative magnitude, the associated DEP mechanisms which, as mentioned above, act in the same direction as their ICEP counterparts, are expected to only have a minor effect on the particle-pair motion.

Acting to induce LOC rotation in a sense opposite to that induced by ICEP, $\bar{F}_y^M$ may, in principle, have a more noticeable effect. This prediction needs, however, to be qualified since the relatively larger ($\approx$7.3%) peak value of the ratio $R_{\bar{B}}$ takes place at radial distances where $\bar{B}$ itself is already substantially diminished (cf. Fig. 5).

Figure 8 is the trajectory pattern of Fig. 6 with the curves marked in red presenting pairs of ICEP and corresponding dipolophoretic (DIP, combined ICEP and DEP) paths (solid and dashed lines, respectively), each pair emanating from the same point. As could be anticipated from the above, the (relatively modest) differences are primarily associated with the transverse motion where both mechanisms have opposing effects, which is manifested in that, owing to DEP effect, when the particles are moving apart the DIP trajectories are somewhat biased towards the direction of the external field (along the X axis). The most conspicuous effect is observed in the path starting near the X axis. Out of the four pairs presented, the particles following this specific track attain the smallest separation distance and spend a relatively large part of their motion under a significant combined effect of transverse DIP motion. Consistently with the discussion of Fig. 6, within the framework of the present model, the resulting bias is indeed larger the closer the path starting point is the X axis.

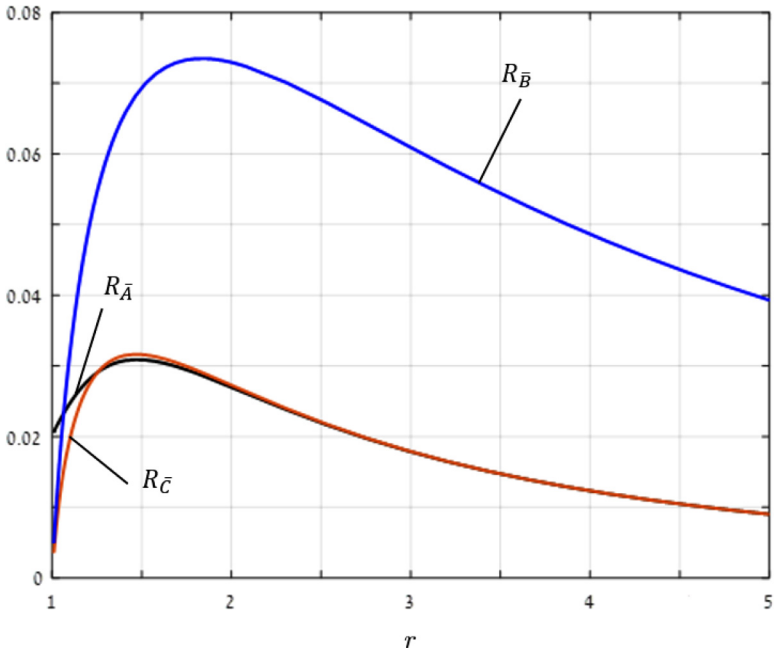

FIG. 7. Variation with r of $R_{\bar{A}}$, $R_{\bar{C}}$, and $R_{\bar{B}}$.

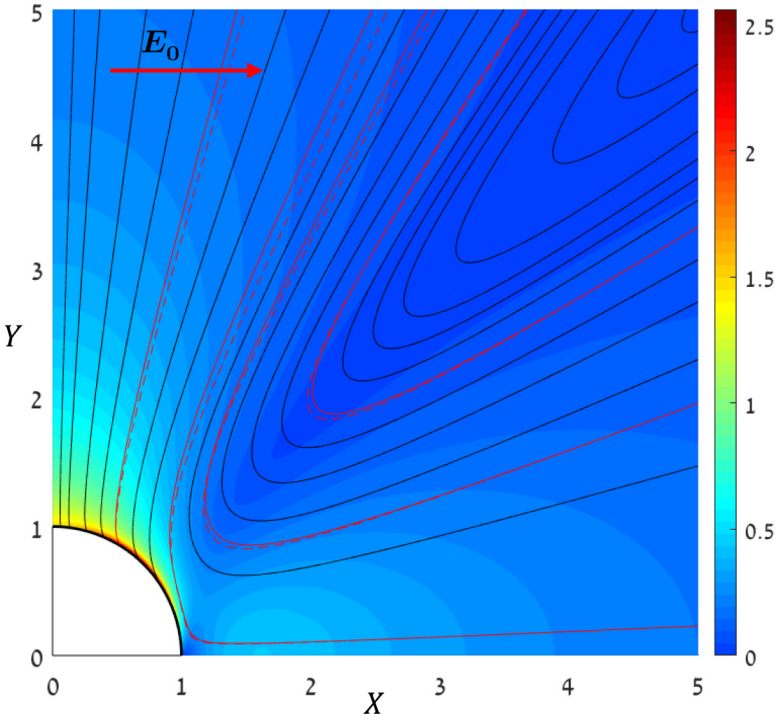

FIG. 8. The trajectory pattern of Fig. 6 with the curves marked in red presenting pairs of ICEP and corresponding dipolophoretic (DIP, combined ICEP and DEP) paths (solid and dashed lines, respectively), each pair emanating from the same point.

As mentioned above, DEP effects associated with the separate contributions of the external-field components are cumulative with the corresponding ICEP contributions, giving rise to larger inward and outward velocities. This is manifested in the DIP trajectories passing through smaller $r_{\min}$, which is clearly visible in the more remote of the pairs presented.

VI. CONCLUDING COMMENTS

We have studied the relative ICEP motion of a pair of ideally polarizable particles freely suspended in an unbounded electrolyte solution under a constant (DC) uniform external field acting in an arbitrary direction relative to the line-of-centers of the particle pair, assuming a thin electric double layer and weak fields. These assumptions together with the 2D geometry facilitate a comprehensive semi-analytic description of particle-pair motion.

As a result of nonlinear interaction between the effects of the external-field components parallel and perpendicular, respectively, to the line of centers, particles experience transient pairing eventually moving away from each other in the general direction perpendicular to the external field. The interaction between external-field components through DEP acts to rotate the LOC in the opposite sense (i.e., clockwise in Fig. 6). While, as demonstrated in Fig. 8, this mechanism only has a relatively minor effect in the present problem for ideally polarizable particles, it is well known that ICEP is rapidly diminishing due to a variety of physical processes (e.g., surface contamination), in which case DEP effect is no longer secondary and may lead to permanent 'chaining' [9].

The present analysis involves the assumptions of thin EDL and weak fields. The former safely applies to microparticles (except for extremely dilute electrolyte solutions or nearly touching particles). Furthermore, it can, in principle, be relaxed (e.g., for nanoparticles) via application of the general method presented for weak fields and small Peclet numbers in Ref. [10]. The weak-field approximation requires that the product $E_0' a'$ be small relative to the thermal potential (typically $\approx$25 mV). While this requirement is safely satisfied for nanoparticles, it may not be the case in a variety of applications involving microparticles. This, in turn, results in the emergence of significant (nonuniform) surface conduction and accompanying bulk-concentration polarization. Relaxation of the weak-field assumption thus necessitates the incorporation of these physical phenomena into the model, which involves challenging issues on both the conceptual and technical levels [22,23].

APPENDIX: THE COEFFICIENTS $A(\alpha_0, \beta)$, $B(\alpha_0, \beta)$ AND $C(\alpha_0, \beta)$

$$\mathrm{A}(\alpha_0,\beta) = -\left[2\sum_{n=1}^{\infty} n e^{-n\alpha_0}\tanh n\alpha_0 \sin n\beta + \frac{\sinh\alpha_0 \sin\beta}{(\cosh\alpha_0 - \cos\beta)^2}\right] \times\left[2\sum_{n=1}^{\infty} e^{-n\alpha_0}\tanh n\alpha_0 (e^{-n\alpha_0} - \cos n\beta) + \left(\coth\alpha_0 - \frac{\sinh\alpha_0}{\cosh\alpha_0 - \cos\beta}\right)\right], \tag{A1}$$

$$\begin{aligned}\mathrm{B}(\alpha_0,\beta) = &\left[2\sum_{n=1}^{\infty} n e^{-n\alpha_0}\coth n\alpha_0 \cos n\beta + \frac{\cosh\alpha_0\cos\beta - 1}{(\cosh\alpha_0 - \cos\beta)^2}\right] \times\left[2\sum_{n=1}^{\infty} e^{-n\alpha_0}\tanh n\alpha_0 (e^{-n\alpha_0} - \cos n\beta) + \left(\coth\alpha_0 - \frac{\sinh\alpha_0}{\cosh\alpha_0 - \cos\beta}\right)\right] \\ &+\left[2\sum_{n=1}^{\infty} e^{-n\alpha_0}\coth n\alpha_0 \sin n\beta + \frac{\sin\beta}{\cosh\alpha_0 - cos\beta}\right] \times\left[2\sum_{n=1}^{\infty} n e^{-n\alpha_0}\tanh n\alpha_0 \sin n\beta + \frac{\sinh\alpha_0 \sin\beta}{(\cosh\alpha_0 - \cos\beta)^2}\right],\end{aligned} \tag{A2}$$

and

$$C(\alpha_0, \beta) = -\left[2\sum_{n=1}^{\infty} e^{-n\alpha_0} \coth n\alpha_0 \sin n\beta + \frac{\sin\beta}{\cosh\alpha_0 - \cos\beta}\right] \times \left[2\sum_{n=1}^{\infty} n e^{-n\alpha_0} \coth n\alpha_0 \cos n\beta + \frac{\cosh\alpha_0 \cos\beta - 1}{(\cosh\alpha_0 - \cos\beta)^2}\right]. \tag{A3}$$

[1] T. M. Squires and M. Z. Baznat, Induced-charge electro-osmosis, J. Fluid Mech. **509**, 217 (2004).

[2] T. M. Squires and M. Z. Bazant, Breaking symmetries in induced - charge electro-osmosis and electrophoresis, J. Fluid Mech. **560**, 65 (2006).

[3] A. M. Boymelgreen and T. Miloh, A theoretical study of induced-charge dipolophoresis of ideally polarizable asymmetrically slipping Janus particles, Phys. Fluids **23**, 072007 (2011).

[4] H. Zhao and H. H. Bau, On the effect of induced electro-osmosis on a cylindrical particle next to a surface, Langmuir **23**, 4053 (2007).

[5] M. Abu Hamed and E. Yariv, Boundary-induced electrophoresis of uncharged conducting particles: Near-contact approximation, Proc. R. Soc. London A **465**, 1939 (2009).

[6] D. Saintillan, E. Darve, and E. S. G. Shaqfeh, Hydrodynamic interactions in the induced - charge electrophoresis of colloidal rod dispersions, J. Fluid Mech. **563**, 223 (2006).

[7] D. Saintillan, Nonlinear interactions in electrophoresis of ideally polarizable particles, Phys. Fluids **20**, 067104 (2008).

[8] J. S. Park and D. Saintillan, Dipolophoresis in large - scale suspensions of ideally polarizable spheres, J. Fluid Mech. **662**, 66 (2010).

[9] J. S. Park and D. Saintillan, From diffusive motion to local aggregation: Effect of surface contamination in dipolophoresis, Soft Matter **7**, 10720 (2011).

[10] T. Miloh, Dipolophoresis of interacting conducting nano-particles of finite electric double layer thickness, Phys. Fluids **23**, 122002 (2011).

[11] A. Ramos, P. García-Sánchez, and H. Morgan, AC electrokinetics of conducting microparticles: A review, Curr. Opin. Colloid Interface Sci. **24**, 79 (2016).

[12] S. Kang, Two-dimensional dipolophoretic motion of a pair of ideally polarizable particles under a uniform electric field, Eur. J. Mech. B-Fluids **41**, 66 (2013).

[13] H. Feng, T. N. Wong, and Marcos, Pair interactions in induced charge electrophoresis of conducting cylinders, Int. J. Heat and Mass Transfer **88**, 674 (2015).

[14] P. Moon and D. E. Spencer, *Field Theory Handbook*, 2nd ed. (Springer, Berlin, 1971).

[15] H. J. Keh, K. D. Horng, and J. Kuo, Boundary effects on electrophoresis of colloidal cylinders, J. Fluid Mech. **231**, 211 (1991).

[16] E. Yariv, Induced-charge electrophoresis of nonspherical particles, Phys. Fluids **17**, 051702 (2005).

[17] I. S. Gradshteyn and I. M. Ryzhik, in *Tables of Integrals, Series, and Products*, 8th ed., edited by D. Zwillinger and V. Moll (Academic, New York, 2014).

[18] G. B. Jeffery, Plane stress and plane strain in bipolar co-ordinates, Philos. Trans. R. Soc. London A **221**, 265 (1921).

[19] G.B. Jeffery, The rotation of two circular cylinders in a viscous fluid, Proc. R. Soc. London A **101**, 169 (1922).

[20] S. Wakiya, Application of bipolar coordinates to the two-dimensional creeping motion of a liquid. II. Some problems for two circular cylinders in viscous fluid, J. Phys. Soc. Japan **39**, 1603 (1975).

[21] J. Happel and H. Brenner, *Low Reynolds Number Hydrodynamics: With Special Applications to Particulate Media* (Martinus Nijhoff, The Hague, 1983).

[22] O. Schnitzer and E. Yariv, Macroscale description of electrokinetic flows at large zeta potentials: Nonlinear surface conduction, Phys. Rev. E **86**, 021503 (2012).

[23] O. Schnitzer and E. Yariv, Induced-charge electro-osmosis beyond weak fields, Phys. Rev. E **86**, 061506 (2012).